Tribology International 164 (2021) 107200

Contents lists available at ScienceDirect

Tribology International

journal homepage: www.elsevier.com/locate/triboint

Inverse determination of sliding surface temperature based on measurements by thermocouples with account of their thermal inertia

Oleksii Nosko *, Yurii Tsybrii

Bialystok University of Technology, Faculty of Mechanical Engineering, ul. Wiejska 45C, Bialystok 15-351, Poland

ARTICLE INFO

Keywords:
Sliding
Frictional heating
Contact temperature
Numerical analysis

ABSTRACT

This study developed an inverse heat conduction algorithm to determine temperature at a sliding surface taking account of thermocouple thermal inertia. The direct heat conduction problem was solved analytically based on the Laplace integral transform approach. The inverse algorithm was applied to the problem of friction of a brake material against a steel. The experiments were conducted on a pin-on-disc tribometer for three short-time sliding regimes: velocity step, acceleration and deceleration. Temperature in the pin sample was measured by two identical miniature thermocouples installed at different distances from the friction surface. It was found that the two inverse surface temperatures agree well between each other. The inverse algorithm allows predicting the contact temperature measured by infrared thermography with accuracy 5–7%.

1. Introduction

Design of a new device or testing of an existing one may require the knowledge of temperatures and heat fluxes at the interfaces between its components and at its boundary with the environment. This knowledge is of critical importance in aerospace engineering [1], chemical engineering [2], mechanical engineering [3], metallurgical engineering [4], power engineering [5], safety engineering [6], etc. In many practical situations, thermal measurements cannot be performed directly in the interfacial region. Installation of a thermal sensor or a group of sensors may distort the processes under consideration. There may be extreme conditions capable of destroying the thermal sensor or deteriorating its performance. This leads to the necessity of applying inverse heat transfer methods that aim at finding functions and parameters incorporated into the thermal boundary conditions of a heat transfer system based on the temperature data obtained for some interior points (Beck et al. [7]).

Thermal problem of friction belongs to the class of contact heat transfer problems in which reliable and accurate measurements of temperatures and heat fluxes present certain technical difficulties. Application of infrared thermography is substantially limited due to the fact that the friction components are generally not transparent. Employment of a thermocouple requires its installation in one of the friction components so that its measuring junction is located as close as possible or even exposed to the friction surface. Involvement of the measuring junction in friction distorts the temperature field in its vicinity and, moreover, may result in its destruction. Special contact sensor techniques, such as thin-film thermocouples (Kennedy et al. [8]) and grindable thermocouples (Nosko et al. [9]), are limited in application to a certain class of friction materials. Thereby, the inverse heat transfer approach looks to be a natural candidate for estimation of temperatures and heat fluxes at a sliding interface.

A number of studies have been devoted to the thermal characterisation of sliding surfaces using various inverse heat transfer methods. Chen et al. [10] developed an inverse algorithm based on the conjugate gradient method and discrepancy principle to estimate the specific power of heat generation at the sliding interface of cylindrical bars. Wang et al. [11] applied a similar approach to the friction system consisting of a semispace and a plane-parallel layer. Quéméner et al. [12] presented a branch eigenmodes reduction method capable of identifying the heat flux dissipated in a brake disc rotating at variable speed. Chen and Yang [13] applied an inverse algorithm to determine the specific power of heat generation at the sliding interface of a semispace and a semispace covered by a layer. Yang and Chen [14] made use of the Lagrange multipliers method and conjugate gradient method to reconstruct the heat flux passing into a car brake disc. Ghadimi et al. [15] developed an inverse algorithm based on a back propagation neural network and a sequential function specification technique to estimate the heat flux absorbed by a locomotive brake disc. Bauzin et al. [16] performed an inverse estimation of the heat flux generated by friction in an aircraft brake. Bauzin et al. [17] also applied an inverse algorithm for identifying the specific power of generation of friction heat and the

* Corresponding author.
E-mail address: o.nosko@pb.edu.pl (O. Nosko).

https://doi.org/10.1016/j.triboint.2021.107200
Received 6 April 2021; Received in revised form 27 June 2021; Accepted 20 July 2021
Available online 27 July 2021

Nomenclature

erfc(•)	complementary error function
exp(•)	exponential function
h	distance between measuring junction and surface, m
i	imaginary unit, $i = \sqrt{-1}$
k	thermal diffusivity, m^2/s
q	surface heat flux, W/m^2
q_{max}	maximum surface heat flux, W/m^2
q_Σ	specific power of heat generation at sliding contact, W/m^2
s	Laplace transform parameter
t	time variable, s
t^*	heating duration, s
x	spatial coordinate, m
C	heat capacity of measuring junction, J/°C
Fo	dimensionless time variable, $Fo = kt/h^2$
Fo^*	dimensionless heating duration, $Fo^* = kt^*/h^2$
K	thermal conductivity, W/(m °C)
Q	dimensionless surface heat flux, $Q = q/q_{max}$
R	thermal resistance of intermediate layer, °C/W
T	temperature, °C
T_h	temperature at $x = h$, °C
T_m	measured temperature, °C
$T_m^{(j)}$	temperature measured by jth thermocouple, °C
T_s	temperature at surface $x = 0$, °C
$T_s^{(j)}$	inverse surface temperature corresponding to jth thermocouple, °C
ε	deviation of maximum ϑ_m from maximum ϑ_s, %
ϑ	dimensionless temperature, $\vartheta = KT/(hq_{max})$
ϑ_h	dimensionless temperature at $\xi = 1$
ϑ_m	dimensionless measured temperature, $\vartheta_m = KT_m/(hq_{max})$
ϑ_s	dimensionless surface temperature
ξ	dimensionless spatial coordinate, $\xi = x/h$
π	Pi number, $\pi \approx 3.14$
σ_m	dimensionless standard deviation of thermocouple noise
σ_s	dimensionless standard deviation of ϑ_s from noise-free solution
τ	time constant of thermocouple, s
ΔFo	dimensionless time step
Θ	dimensionless time constant, $\Theta = k\tau/h^2$
Ω	noise sensitivity of inverse algorithm
$\mathscr{L}[\bullet]$	Laplace transform operator
$\widetilde{\blacksquare}$	Laplace transform image
MRAD	mean relative absolute difference

parameters responsible for its partition between the friction components.

When a thermocouple is used to measure temperature in a friction system, its measuring junction is placed inside one of the friction components. For this purpose, a blind hole is made in the friction component by means of drilling or other technique. The measuring junction of the thermocouple is inserted into the hole and is normally attached to its bottom face. The macroscopic shape of the measuring junction does not match that of the hole bottom face, which implies an air gap between them. There are, in addition, microscopic air voids due to the roughness of the contacting surfaces. Sometimes, the hole is filled in with a thermal paste to eliminate the air. Thereby, the air medium or/and thermal paste form an intermediate layer between the measuring junction and friction component. The thermal resistance of this layer results in a substantial increase in the thermal inertia of the thermocouple, which affects its dynamic behaviour under a non-stationary regime. Analysis of [10–17] and other literature sources shows, however, that the inverse heat transfer methods and algorithms developed for solving thermal problems of friction take no account of the thermocouple dynamics.

The dynamic behaviour of a thermocouple is often described using a first-order model. Woodbury [18] developed an inverse algorithm incorporating a thermocouple first-order model to evaluate the influence of the thermocouple time constant on predictions of the surface heat flux in the form of a triangular impulse. Tagawa and Ohta [19] developed a theoretical basis for application of two thermocouples with fluctuating time constants to measuring gas temperature in combustion and demonstrated its validity by measurements in a combustion wind tunnel. Augustin et al. [20] performed finite-element analysis of the static and dynamic errors of a thermocouple sensor built into a turbocharger, which enabled more accurate prediction of the fluid temperature. Frankel and Chen [21] proposed a methodology for validation of a thermocouple model by experimental reconstruction of the thermal impulse response function and demonstrated its efficiency on example of a first-order model. Following the mentioned studies, the purpose of the present study was to develop and validate an inverse heat conduction algorithm based on a thermocouple first-order model for accurate prediction of non-stationary temperature at a sliding surface.

2. Model of the thermocouple measuring junction

Consider a body that occupies the domain $x > 0$ and is characterised by thermal conductivity K and thermal diffusivity k, as illustrated in Fig. 1. The body is heated at its surface $x = 0$ by heat flux q changing in time t. Temperature $T(x,t)$ in the body is then defined by the heat conduction equation

$$\frac{\partial T}{\partial t} = k\frac{\partial^2 T}{\partial x^2}, \quad x > 0, \quad 0 < t < t^* \tag{1}$$

initial condition

$$T|_{t=0} = 0 \tag{2}$$

boundary condition

$$-K\left.\frac{\partial T}{\partial x}\right|_{x=0} = q(t) = q_{max}Q(t) \tag{3}$$

and condition of zero disturbance at infinity

$$\left.\frac{\partial T}{\partial x}\right|_{x\to\infty} = 0 \tag{4}$$

where t^* is the heating duration; q_{max} is the maximum value of the heat flux q; $Q = q/q_{max}$ is the dimensionless heat flux, $0 \le Q \le 1$. The temperature of the body at the surface $x = 0$ is denoted by T_s. Note that the zero initial condition of Eq. (2) is not restrictive and is accepted for shorter notation.

Now let a thermocouple be installed in the body so that its measuring junction is located at distance h from the surface. The size of the measuring junction is small compared to h. Assume that the temperature $T_m(t)$ of the measuring junction is uniformly distributed over its volume. The measuring junction can then be modelled as a point of heat capacity C. The thermal contact between the measuring junction and body is imperfect due to the presence of an intermediate layer with thermal resistance R. Accordingly, the thermocouple response to the temperature T_h of the body at $x = h$ obeys the following heat balance equation:

$$CdT_m = \frac{T_h - T_m}{R}dt$$

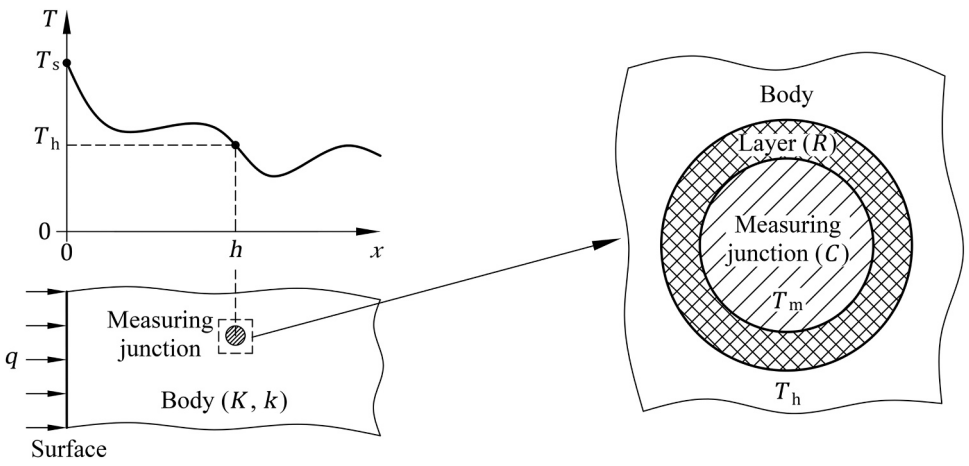

Fig. 1. Model of the thermocouple measuring junction.

or

$$\tau\frac{dT_{\mathrm{m}}}{dt}+T_{\mathrm{m}}=T_{\mathrm{h}} \tag{5}$$

where $\tau = CR$ is the time constant of the thermocouple.

Specification of the following initial condition completes the description of the problem:

$$T_{\mathrm{m}}|_{t=0}=0 \tag{6}$$

Thereby, Eqs. (1)–(6) define the relationship between the heat flux q and measured temperature T_{m} in dependence on the parameters K, k, h and τ.

3. Analytical solution of the direct problem

Introduction of the dimensionless variables

$$\xi=\frac{x}{h},\quad \mathrm{Fo}=\frac{kt}{h^2},\quad \vartheta=\frac{KT}{hq_{\max}},\quad \vartheta_{\mathrm{m}}=\frac{KT_{\mathrm{m}}}{hq_{\max}}$$

and parameters

$$\mathrm{Fo}^{*}=\frac{kt^{*}}{h^2},\quad \Theta=\frac{k\tau}{h^2}$$

allows representing Eqs. (1)–(6) in the dimensionless form

$$\frac{\partial\vartheta}{\partial\mathrm{Fo}}=\frac{\partial^2\vartheta}{\partial\xi^2},\quad \xi>0,\quad 0<\mathrm{Fo}<\mathrm{Fo}^{*};$$

$$-\left.\frac{\partial\vartheta}{\partial\xi}\right|_{\xi=0}=Q(\mathrm{Fo});$$

$$\left.\frac{\partial\vartheta}{\partial\xi}\right|_{\xi\to\infty}=\vartheta|_{\mathrm{Fo}=0}=0;$$

$$\Theta\frac{d\vartheta_{\mathrm{m}}}{d\mathrm{Fo}}+\vartheta_{\mathrm{m}}=\vartheta|_{\xi=1};$$

$$\vartheta_{\mathrm{m}}|_{\mathrm{Fo}=0}=0 \tag{7}$$

Further, application of the Laplace integral transform $\mathscr{L}$ with respect to the time variable Fo (Doetsch [22])

$\widetilde{\vartheta}(\xi,s)=\mathscr{L}[\vartheta(\xi,\mathrm{Fo})]$;
$\widetilde{\vartheta}_{\mathrm{m}}(s)=\mathscr{L}[\vartheta_{\mathrm{m}}(\mathrm{Fo})]$;
$\widetilde{Q}(s)=\mathscr{L}[Q(\mathrm{Fo})]$

describes Eq. (7) in the space of images as

$$\frac{\partial^2\widetilde{\vartheta}}{\partial\xi^2}-s\widetilde{\vartheta}=0,\xi>0;$$

$$-\left.\frac{\partial\widetilde{\vartheta}}{\partial\xi}\right|_{\xi=0}=\widetilde{Q}(s);$$

$$\left.\frac{\partial\widetilde{\vartheta}}{\partial\xi}\right|_{\xi\to\infty}=0;$$

$$\widetilde{\vartheta}_{\mathrm{m}}=\frac{\widetilde{\vartheta}|_{\xi=1}}{\Theta s+1} \tag{8}$$

where s is the Laplace transform parameter.

The solution of Eq. (8) can be easily found as

$$\widetilde{\vartheta}(\xi,s)=\widetilde{Q}(s)\frac{\exp\{-\xi\sqrt{s}\}}{\sqrt{s}};$$

$$\widetilde{\vartheta}_{\mathrm{s}}(s)=\widetilde{\vartheta}|_{\xi=0}=\frac{\widetilde{Q}(s)}{\sqrt{s}};$$

$$\widetilde{\vartheta}_{\mathrm{h}}(s)=\widetilde{\vartheta}|_{\xi=1}=\widetilde{Q}(s)\frac{\exp\{-\sqrt{s}\}}{\sqrt{s}};$$

$$\widetilde{\vartheta}_{\mathrm{m}}(s)=\widetilde{Q}(s)\frac{\exp\{-\sqrt{s}\}}{\sqrt{s}(\Theta s+1)} \tag{9}$$

whence one obtains the following relationship

$$\widetilde{\vartheta}_{\mathrm{m}}(s)=\widetilde{Q}(s)\widetilde{\varphi}(s)=\widetilde{\vartheta}_{\mathrm{s}}(s)\widetilde{\psi}(s) \tag{10}$$

with the functions $\widetilde{\varphi}$ and $\widetilde{\psi}$ given by

$$\widetilde{\varphi}(s)=\frac{\exp\{-\sqrt{s}\}}{\sqrt{s}(\Theta s+1)} \tag{11}$$

and

$$\widetilde{\psi}(s)=\frac{\exp\{-\sqrt{s}\}}{\Theta s+1} \tag{12}$$

Based on the known transforms (Carslaw and Jaeger [23], p. 495, 496)

$$\mathscr{L}^{-1}\left[\frac{\exp\{-\xi\sqrt{s}\}}{\sqrt{s}(s-b)}\right]=\frac{\exp\{b\mathrm{Fo}\}}{2\sqrt{b}}$$
$$\left(\exp\left\{-\xi\sqrt{b}\right\}\mathrm{erfc}\left\{\frac{\xi}{2\sqrt{\mathrm{Fo}}}-\sqrt{b\mathrm{Fo}}\right\}\right.$$
$$\left.-\exp\left\{\xi\sqrt{b}\right\}\mathrm{erfc}\left\{\frac{\xi}{2\sqrt{\mathrm{Fo}}}+\sqrt{b\mathrm{Fo}}\right\}\right)$$

and

$$\mathscr{L}^{-1}\left[\frac{\exp\{-\xi\sqrt{s}\}}{s-b}\right]=\frac{\exp\{b\mathrm{Fo}\}}{2}$$
$$\left(\exp\left\{-\xi\sqrt{b}\right\}\mathrm{erfc}\left\{\frac{\xi}{2\sqrt{\mathrm{Fo}}}-\sqrt{b\mathrm{Fo}}\right\}\right.$$
$$\left.+\exp\left\{\xi\sqrt{b}\right\}\mathrm{erfc}\left\{\frac{\xi}{2\sqrt{\mathrm{Fo}}}+\sqrt{b\mathrm{Fo}}\right\}\right)$$

at $\xi=1$ and $b=-\Theta^{-1}$, the images of Eq. (11) and Eq. (12) are represented as

$$\varphi(\mathrm{Fo})=\frac{\exp\{-\mathrm{Fo}/\Theta\}}{2i\sqrt{\Theta}}$$
$$\left(\exp\left\{-\frac{i}{\sqrt{\Theta}}\right\}\mathrm{erfc}\left\{\frac{1}{2\sqrt{\mathrm{Fo}}}-i\frac{\sqrt{\mathrm{Fo}}}{\sqrt{\Theta}}\right\}\right.$$
$$\left.-\exp\left\{\frac{i}{\sqrt{\Theta}}\right\}\mathrm{erfc}\left\{\frac{1}{2\sqrt{\mathrm{Fo}}}+i\frac{\sqrt{\mathrm{Fo}}}{\sqrt{\Theta}}\right\}\right) \tag{13}$$

and

$$\psi(\mathrm{Fo})=\frac{\exp\{-\mathrm{Fo}/\Theta\}}{2\Theta}$$
$$\left(\exp\left\{-\frac{i}{\sqrt{\Theta}}\right\}\mathrm{erfc}\left\{\frac{1}{2\sqrt{\mathrm{Fo}}}-i\frac{\sqrt{\mathrm{Fo}}}{\sqrt{\Theta}}\right\}\right.$$
$$\left.+\exp\left\{\frac{i}{\sqrt{\Theta}}\right\}\mathrm{erfc}\left\{\frac{1}{2\sqrt{\mathrm{Fo}}}+i\frac{\sqrt{\mathrm{Fo}}}{\sqrt{\Theta}}\right\}\right) \tag{14}$$

Here $i=\sqrt{-1}$ is the imaginary unit.

Taking account of Eqs. (10), (13), (14) allows expressing the measured temperature ϑ_m in the form of convolutions

$$\vartheta_\mathrm{m}(\mathrm{Fo})=\int_0^{\mathrm{Fo}}Q(\mathrm{Fo}-\varsigma)\varphi(\varsigma)d\varsigma=\int_0^{\mathrm{Fo}}\vartheta_\mathrm{s}(\mathrm{Fo}-\varsigma)\psi(\varsigma)d\varsigma \tag{15}$$

If the heat flux Q is defined as a polynomial of order n with coefficients a_j, i.e.

$$Q(\mathrm{Fo})=\sum_{j=0}^{n}a_j\mathrm{Fo}^j \tag{16}$$

then Eq. (15) transforms into

$$\vartheta_\mathrm{m}(\mathrm{Fo})=\sum_{j=0}^{n}j!a_j\varphi_j(\mathrm{Fo}) \tag{17}$$

where the function φ_j is determined by repeated integration

$$\varphi_j(\mathrm{Fo})=\underbrace{\int_0^{\mathrm{Fo}}\cdots\int_0^{\mathrm{Fo}}}_{j+1}\varphi(\varsigma)\underbrace{d\varsigma\ldots d\varsigma}_{j+1}$$

The original of the surface temperature is easily expressed from Eq. (9) as

$$\vartheta_\mathrm{s}(\mathrm{Fo})=\int_0^{\mathrm{Fo}}\frac{Q(\mathrm{Fo}-\varsigma)}{\sqrt{\pi\varsigma}}d\varsigma \tag{18}$$

or, if, in addition, Eq. (16) holds, (Carslaw and Jaeger [23], p.494)

$$\vartheta_\mathrm{s}(\mathrm{Fo})=\frac{1}{\sqrt{\pi}}\sum_{j=0}^{n}\frac{j!2^{j+1}a_j}{(2j+1)!!}\mathrm{Fo}^{j+1/2} \tag{19}$$

Thereby, the temperatures ϑ_m and ϑ_s can be determined using respective Eq. (15) and Eq. (18) for an arbitrary heat flux Q or using respective Eq. (17) and Eq. (19) for Q given by Eq. (16).

4. Influence of the heating duration and time constant

The behaviour of the dimensionless temperatures ϑ_s, ϑ_h and ϑ_m depends on the regime specified by the heat flux function Q and heating duration Fo^*. Besides, the behaviour of ϑ_m is affected by the time constant Θ. Fig. 2 presents the curves of ϑ_s, ϑ_h and ϑ_m for a linearly decreasing heat flux. The temperature ϑ_h at $\xi=1$ changes with some delay compared to ϑ_s, which is caused by the propagation of heat from the surface $\xi=0$ to the distance $\xi=1$. The measured temperature ϑ_m reacts with even more delay due to the thermal inertia of the thermocouple.

Introduce and analyse the deviation ε of the maximum value of the measured temperature ϑ_m from the maximum value of the surface temperature ϑ_s reached during the heating process:

$$\varepsilon=\left(1-\frac{\max\vartheta_\mathrm{m}}{\max\vartheta_\mathrm{s}}\right)100\%$$

Fig. 3 shows the contour line of $\varepsilon=1\%$ in the plane (Fo^*,Θ) for the following heating regimes: constant heat flux $Q=1$, increasing heat flux $Q=\mathrm{Fo}/\mathrm{Fo}^*$ and decreasing heat flux $Q=1-\mathrm{Fo}/\mathrm{Fo}^*$. It is seen that the presented contour lines are qualitatively similar for all regimes under consideration. In the region of $\varepsilon<1\%$, ϑ_m, ϑ_h and ϑ_s practically coincide, i.e. the measured temperature ϑ_m follows the surface temperature ϑ_s with a negligibly small deviation. On the contrary, ϑ_m may substantially differ from ϑ_s in the region of $\varepsilon>1\%$, which is the subject of the present study.

Fig. 4 shows the contour lines of ε for a constant heat flux. At Θ of order 10^{-1} and below, ϑ_m is almost identical to ϑ_h, and ε is governed solely by Fo^*. On the other hand, at Θ of order 10 and above, the difference between ϑ_m and ϑ_h increases with increasing Θ, and ε depends on both Fo^* and Θ.

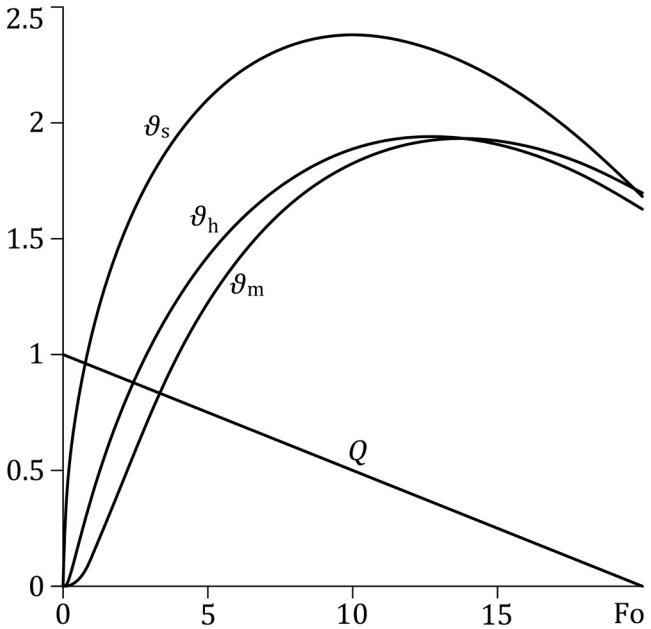

Fig. 2. Dimensionless temperatures ϑ_s, ϑ_h and ϑ_m for $Q=1-\mathrm{Fo}/\mathrm{Fo}^*$ at $\mathrm{Fo}^*=20$ and $\Theta=1$.

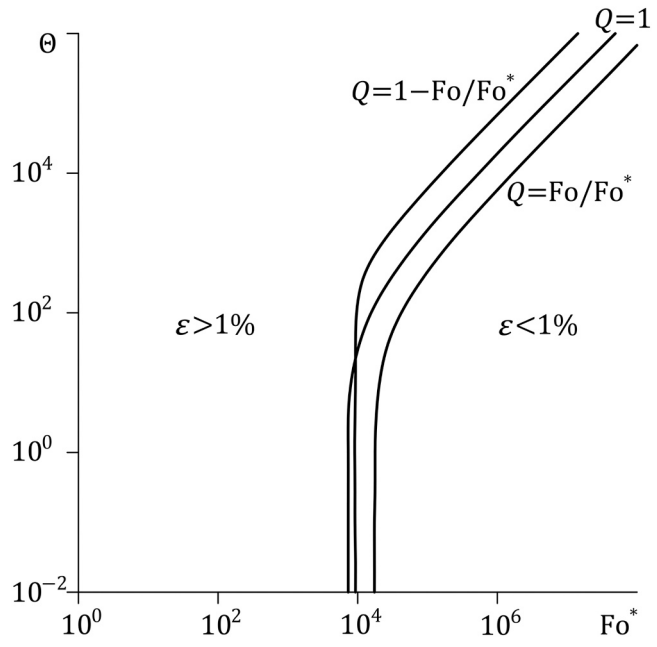

Fig. 3. Contour line of $\varepsilon = 1\%$ in the plane (Fo^*, Θ) for different heating regimes.

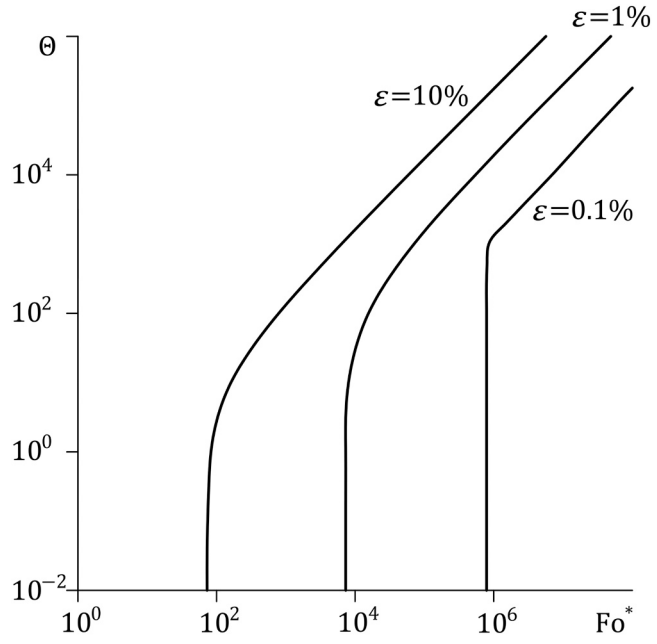

Fig. 4. Contour lines of ε in the plane (Fo^*, Θ) at $Q = 1$.

5. Numerical solution of the inverse problem

The inverse problem implies finding the surface temperature ϑ_s based on the measured temperature ϑ_m according to Eq. (15) that represents a Volterra linear equation of the first kind with a difference kernel. The kernel function $\psi(\mathrm{Fo})$ given by Eq. (14) is not defined at $\mathrm{Fo} = 0$, has a point of maximum and tends to zero at $\mathrm{Fo}\to\infty$, as shown in Fig. 5. At the initial time $\mathrm{Fo} = 0$, it holds that $\vartheta_s = \vartheta_m = 0$ due to Eq. (2) and Eq. (6).

A numerical solution of Eq. (15) can be obtained by applying the method of quadratures. For example, discretisation of time with step $\Delta\mathrm{Fo}$ and approximation of ϑ_s in the nodes $\mathrm{Fo} = \Delta\mathrm{Foj}$ due to the right rectangle rule transform Eq. (15) in the system of linear algebraic

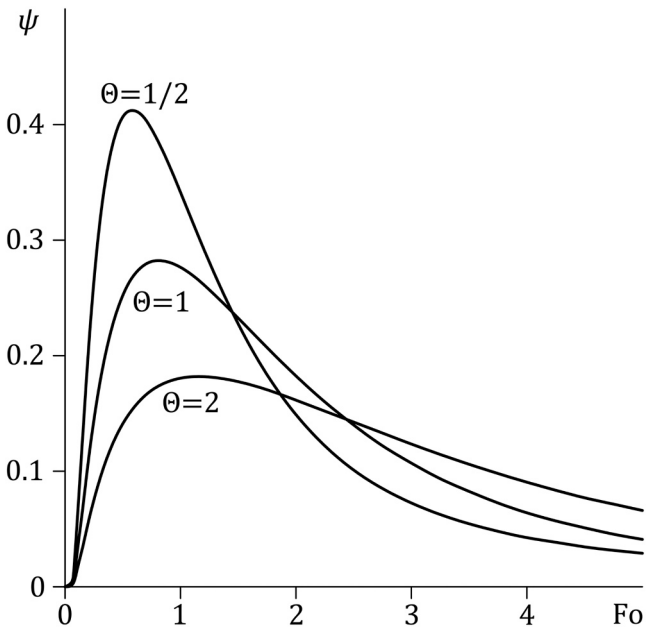

Fig. 5. Kernel function $\psi(\mathrm{Fo})$.

equations

$$\vartheta_m(\Delta\mathrm{Fo}j) = \sum_{l=1}^{j} \vartheta_s(\Delta\mathrm{Fo}l)\Delta\psi_{j-l}$$

which can be solved using the recurrent formula (Stolz [24], Beck [25])

$$\vartheta_s(\Delta\mathrm{Fo}j) = \frac{1}{\Delta\psi_0}\left(\vartheta_m(\Delta\mathrm{Fo}j) - \sum_{l=1}^{j-1} \vartheta_s(\Delta\mathrm{Fo}l)\Delta\psi_{j-l}\right) \tag{20}$$

Here j is the time step number; $\Delta\psi_{\blacksquare}$ is the coefficient calculated by integration of Eq. (14) as follows:

$$\Delta\psi_p = \int_{\Delta\mathrm{Fop}}^{\Delta\mathrm{Fo}(p+1)} \psi(\varsigma)\mathrm{d}\varsigma$$

Specification of the time step $\Delta\mathrm{Fo}$ should be rational. If $\Delta\mathrm{Fo}$ is too small, the inverse solution is unstable, which manifests itself in the occurrence of undesirable oscillations. On the other hand, the approximation of ϑ_s is rough for too large $\Delta\mathrm{Fo}$, resulting in filtering of physically explainable frequencies. Following the natural step regularisation principle (Alifanov [26], p.103–117), $\Delta\mathrm{Fo}$ is set equal to the point of maximum of $\psi(\mathrm{Fo})$.

The validity of the inverse algorithm of Eqs. (14), (20) is substantiated by its comparisons with the direct solution of Eq. (19), as shown in Fig. 6. The values of Fo^* and Θ are characteristic for the experimental study considered in Section 7. It is seen that the inverse algorithm is sufficiently accurate, except for the start interval of time where it underestimates the direct solution.

Application of the inverse algorithm requires specification of the parameters k, h and τ. The thermal diffusivity k is usually determined using one of the well-established experimental techniques. The distance h can be measured directly. As regards the time constant τ, this parameter depends on the shape, size and material of the measuring junction, configuration of the hole where the measuring junction is installed, properties of the intermediate layer, etc. Therefore, its determination usually involves a separate experimental study.

6. Noise robustness of the inverse algorithm

The signal of a thermocouple is affected by the measurement system

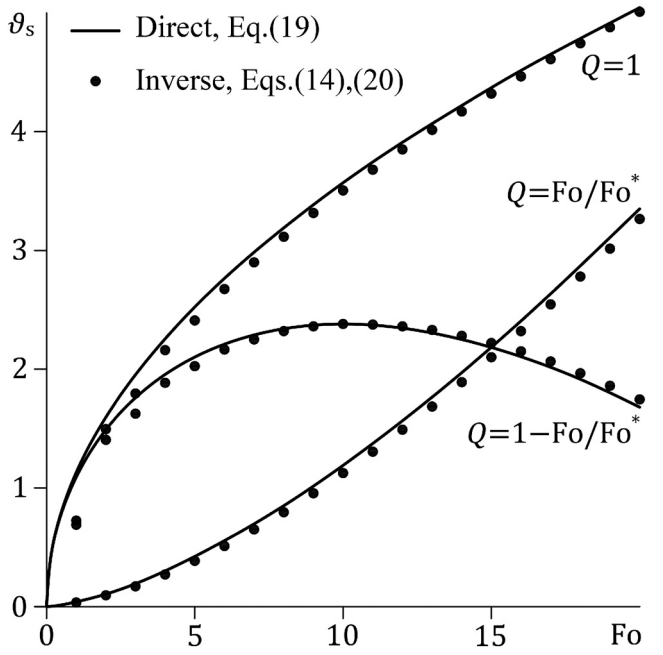

Fig. 6. Comparison of the direct and inverse solutions at $Fo^* = 20$ and $\Theta = 1$.

and environmental electromagnetic field, which results in the occurrence of noise – an undesired component of the signal. The presence of noise may substantially reduce the ability of an inverse heat conduction method to reconstruct the surface temperature or heat flux (Beck et al. [7]).

The noise robustness of the inverse algorithm of Eqs. (14), (20) is investigated by adding noise to the measured temperature ϑ_m and analysing its impact on the inverse surface temperature ϑ_s. The noise obeys a Gaussian distribution with zero mean and standard deviation σ_m. The impact is characterised by the standard deviation σ_s of ϑ_s from the direct solution of Eq. (19). Fig. 7 provides a relevant illustration.

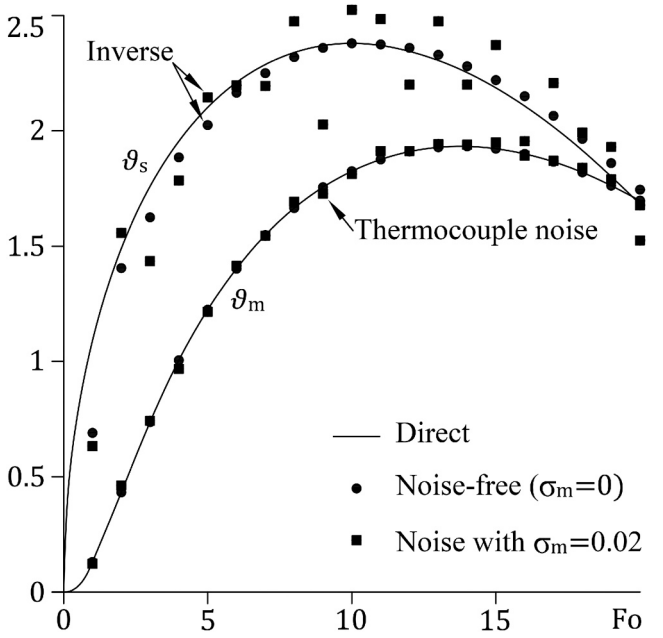

Fig. 7. Impact of the thermocouple noise on the inverse surface temperature ϑ_s for $Q = 1 - Fo/Fo^*$ at $Fo^* = 20$ and $\Theta = 1$.

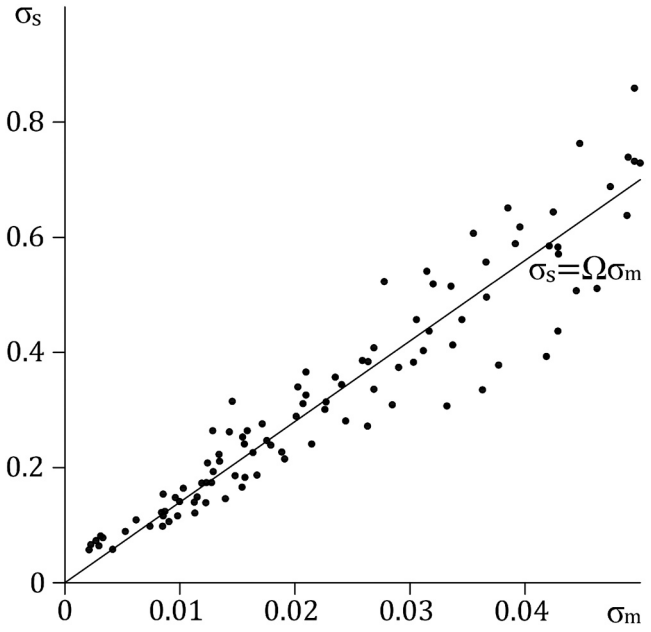

Fig. 8. Typical relationship between σ_m and σ_s for $Q = 1 - Fo/Fo^*$ at $Fo^* = 20$ and $\Theta = 1$.

The statistical relationship between σ_m and σ_s is obtained by multiple simulations, as shown in Fig. 8. There is a fairly good proportional correlation between the quantities. Of practical interest is the ratio σ_s/σ_m that allows estimating σ_s based on an experimentally obtained value of σ_m. With this in mind, the inverse algorithm is characterised by the noise sensitivity Ω defined as the slope coefficient of the least squares fit:

$$\Omega = \sum_j \left(\sigma_m^{(j)}\sigma_s^{(j)}\right) / \sum_j \left(\sigma_m^{(j)}\right)^2$$

where $\sigma_m^{(j)}$ and $\sigma_s^{(j)}$ are the standard deviations corresponding to the jth simulation.

The simulations show that Ω weakly depends on the heating regime.

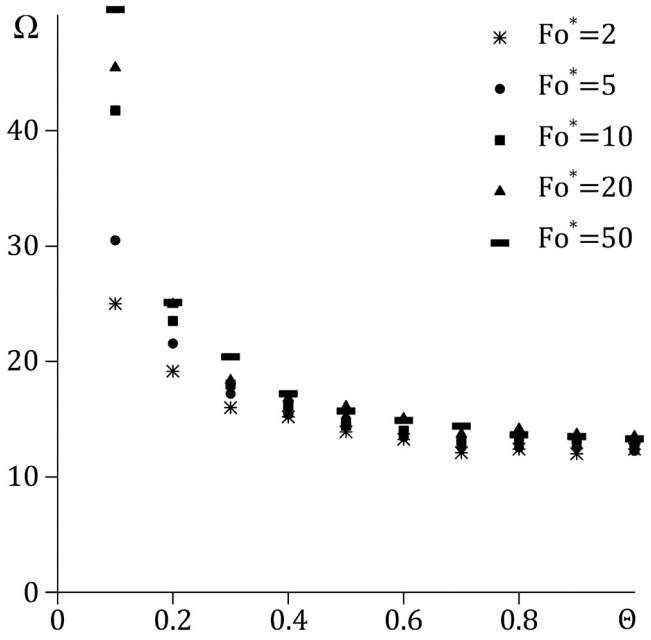

Fig. 9. Typical influence of the heating duration Fo^* and time constant Θ on the noise sensitivity Ω.

Fig. 9 illustrates the influence of the heating duration Fo^* and time constant Θ. Generally, an increase in Fo^* on interval 2–50 leads to an increase in Ω, which is especially noticeable at smaller Θ. On the other hand, as Θ increases on interval 0.1–1, Ω decreases. On the mentioned intervals of variation of Fo^* and Θ, the value of Ω varies between about 12 and 50, i.e. the inverse surface temperature ϑ_s is rather sensitive to the thermocouple noise.

7. Experimental validation

An efficient experimental approach to the reconstruction of temperature or heat flux at the surface of a body is the parallel application of two (or more) identical thermocouples installed in the body at different distances from the surface. The identical thermocouples installed according to the same procedure are expected to have the same time constant τ, as mentioned by Woodbury [18]. The present section applies the mentioned approach along with the inverse algorithm of Eqs. (14), (20) to the problem of friction of a brake material against a steel.

7.1. Experimental set-up

The experiments were performed on a Bruker UMT-2 tribometer equipped with an S23LE rotational motion drive and a DFH-20 force sensor. The pin sample had diameter 8 mm and height 8 mm. The disc sample had diameter 70 mm and thickness 6.5 mm. The average friction radius, i.e. the distance between the axes of the pin and disc samples, was 30 mm.

The pin sample was milled out from a friction pad of a car brake. The material of the friction pad belonged to the class of low-metallic materials. Its thermal diffusivity k was equal to 0.27 mm^2/s. The disc sample was manufactured of 42CrMo4 steel.

Two 0.7 mm diameter blind holes were drilled in the pin sample parallel to its axis on a 6040T4D numerically controlled milling machine. The distance between the axes of the holes was 2.5 mm. Two identical K-type thermocouples 1 and 2 with 0.08 mm diameter bare wires were then installed in the holes, as shown in Fig. 10. Their measuring junctions were attached to the bottom faces of the holes. The distance between the measuring junction and the friction surface was 0.3 mm for the thermocouple 1 and 0.7 mm for the thermocouple 2. The thermocouples were fixed by gluing their wires to the reverse surface of the pin sample.

The temperature signals $T_m^{(1)}$ and $T_m^{(2)}$ from the respective thermocouples 1 and 2 were sampled by a Graphtech GL7000/GL7-HSV data logger at frequency 10 Hz. The signal noise was reduced by a low-pass filter with cutoff frequency 5 Hz. Analysis of the temperature signals obtained under stationary conditions in the absence of friction showed that the noise standard deviation was about 0.03 °C.

The temperature of the pin sample was also measured by a Cedip Titanium 560M infrared thermographic camera with detector spectral range 3.6–5.1 μm, thermal sensitivity 20 mK and resolution 640 × 512 pixels. The emissivity parameter of the camera was set equal to 0.97. The camera was focussed on the visible part of the pin sample, as illustrated in Fig. 11. The spatial resolution of the thermal image was 0.17 mm. The temperature rise T_{IR} of the pin sample averaged over the central visible contact region of 3.4 mm × 0.17 mm was recorded at frequency 10 Hz. The mentioned region is indicated in the enlarged view of the pin-on-disc contact by yellow rectangle.

The sliding duration in each experiment was $t^* = 5$ s. This value corresponded to a short-time heat conduction process in the pin sample (with thermal diffusivity k=0.27 mm^2/s) at which the temperature / heat flux at the reverse surface $x = 8$ mm was more than 10^5 times smaller than the temperature / heat flux at the friction surface $x = 0$ (Carslaw and Jaeger [23], p.75). Thereby, the pin sample could be assumed to be infinitely long, and the boundary condition of Eq. (4) was valid.

The nominal pressure at the sliding contact was 1 MPa. The sliding velocity at the average friction radius varied between 0 and 4 m/s. The chosen values of the nominal contact pressure and maximum sliding velocity provided a narrow range of temperature in the pin sample (of about 20–70 °C), which allowed neglecting the influence of temperature on k.

Fig. 12 presents the time dependency of the specific power q_Σ of heat generation at the sliding contact determined as the product of the measured friction force and sliding velocity divided by the nominal contact area of the pin sample. The regime 'velocity step' implied an increase in q_Σ for about 0.5 s and maintaining its magnitude at a desired level. Note that there were insignificant wave-like variations of q_Σ due to the dynamics of the tribometer. The regime 'acceleration' represented a close to linear increase in q_Σ. The regime 'deceleration' implied an increase in q_Σ for about 1 s and subsequent close to linear decrease in its magnitude.

The pin and disc samples were initially rubbed to provide a uniform distribution of the contact pressure. Then the experiments were done 3 times in each sliding regime. Before each experiment, the pin and disc

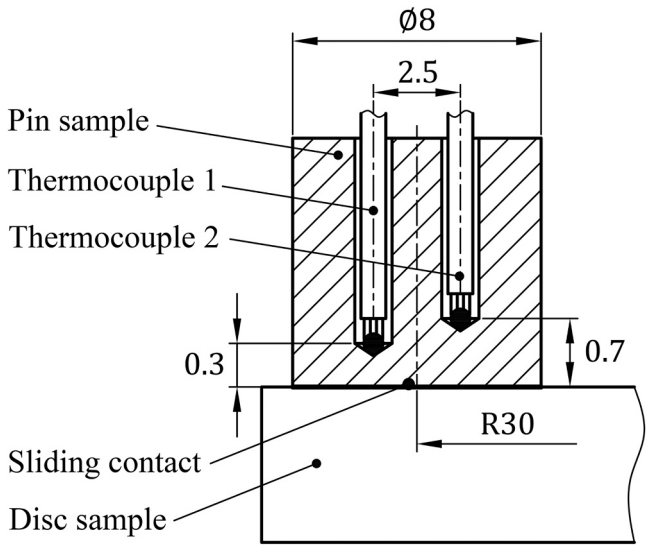

Fig. 10. Schematic of the pin sample in sliding contact with the disc sample.

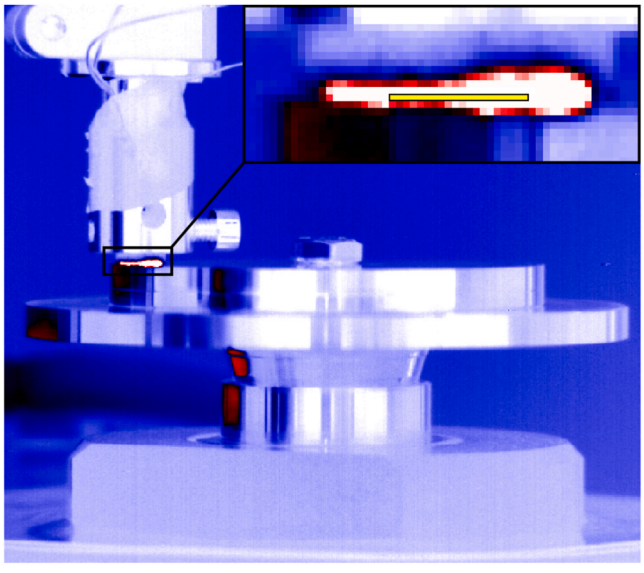

Fig. 11. Thermal image obtained by infrared thermography.

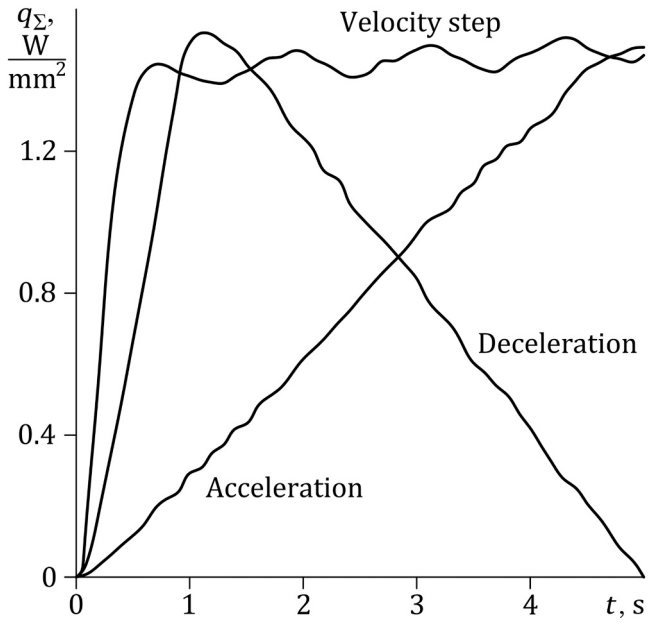

Fig. 12. Specific power q_Σ of heat generation at the sliding contact.

samples cooled down to the room temperature (about 20 °C) and, accordingly, $T_m^{(1)}$, $T_m^{(2)}$ and T_{IR} were equal to zero.

7.2. Estimation of the time constant

The time constant τ was estimated by bringing the friction surface of the pin sample in contact with water at relative temperature $T_s = 39$ °C and analysing the response $T_m^{(1)}$ of the thermocouple 1. The corresponding analytical expression of the measured temperature T_m was obtained by Eq. (15). The value $\tau^* = 0.22$ s of the time constant was found which provided the minimum least squares deviation of T_m from $T_m^{(1)}$. Fig. 13 shows the relevant temperatures. For the sake of comparison, the curve of T_m is also shown for a thermocouple with instantaneous response ($\tau = 0$).

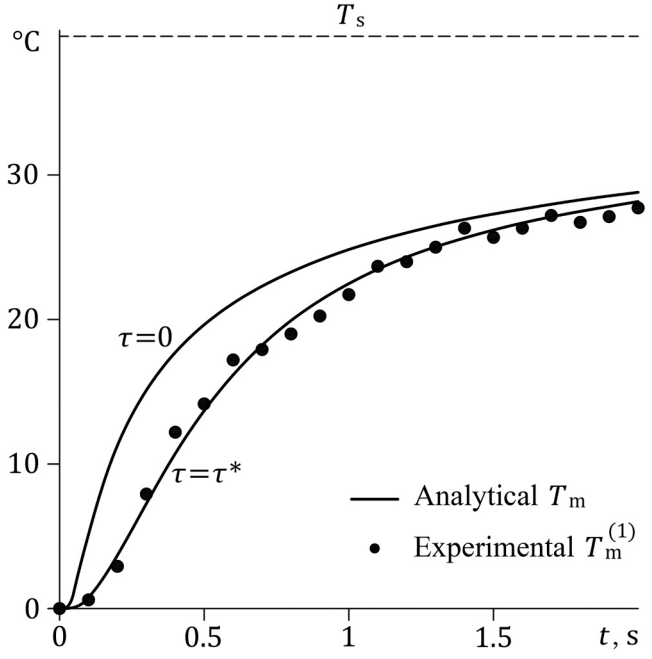

Fig. 13. Response $T_m^{(1)}$ of the thermocouple 1 to a rapid rise of the surface temperature T_s.

7.3. Estimation of the noise sensitivity

The measuring junctions of the thermocouples 1 and 2 were located in the pin sample at different distances from the friction surface. Therefore, the respective values of the dimensionless sliding duration Fo^* and time constant Θ were different. Based on them, the noise sensitivity Ω of the inverse algorithm was estimated for each thermocouple, as presented in Table 1. As mentioned in Section 7.1, the standard deviation of the thermocouple noise was about 0.03 °C. Thereby, the standard deviation of the inverse surface temperature from the noise-free solution was expected to be of order for the thermocouple 1 and for the thermocouple 2.

7.4. Results

The experiment repetitions allow evaluating the repeatability of the thermocouple measurements. Fig. 14 illustrates the temperatures $T_m^{(1)}$ and $T_m^{(2)}$ measured in 3 consecutive experiments. It is seen that the temperature curves agree well between each other for all sliding regimes.

Fig. 15 shows temperature results from the experiments conducted under the three sliding regimes. Thin solid lines indicate the thermocouple temperatures $T_m^{(1)}$ and $T_m^{(2)}$. Thick solid line indicates the temperature rise T_{IR} measured by the infrared camera. The temperatures $T_s^{(1)}$ and $T_s^{(2)}$ of the sliding surface reconstructed by the inverse algorithm of Eqs. (14), (20) are indicated by the respective symbols • and ■.

In the further analysis, the degree of mismatch between two temperature samples X and Y of size n is characterised by the mean relative absolute difference (MRAD) defined as

$$\mathrm{MRAD}(X,Y) = \frac{1}{n}\sum_{j=1}^{n}\frac{|X_j - Y_j|}{X_j}$$

Fig. 15a presents the results obtained for the regime of velocity step. The curves of $T_m^{(1)}$, $T_m^{(2)}$ and T_{IR} exhibit a qualitatively similar behaviour. MRAD between $T_s^{(1)}$ and $T_s^{(2)}$ makes up 6.2%. The values of $T_s^{(1)}$ are close to the curve of T_{IR}. MRAD between T_{IR} and $T_s^{(1)}$ is 4.7%. It is remarkable that $T_s^{(1)}$ reproduces the wave-like variations of the specific power q_Σ shown in Fig. 12.

Further, Fig. 15b corresponds to the regime of acceleration. The curves of $T_m^{(1)}$, $T_m^{(2)}$ and T_{IR} represent almost linear dependencies. $T_s^{(1)}$ and $T_s^{(2)}$ practically coincide, with MRAD of 5.2%. The values of $T_s^{(1)}$ and $T_s^{(2)}$ lie close to the curve of T_{IR}. MRAD between T_{IR} and $T_s^{(1)}$ is 6.1%.

Finally, Fig. 15c shows the results obtained for the regime of deceleration. The values of $T_s^{(1)}$ and $T_s^{(2)}$ are close between each other, with MRAD of 6.3%. They describe well the behaviour of T_{IR} including the location and magnitude of its peak. MRAD between T_{IR} and $T_s^{(1)}$ is 7.1%. On the end interval, $T_s^{(1)}$ and $T_s^{(2)}$ are slightly lower than $T_m^{(1)}$ and $T_m^{(2)}$. This may be caused by that the specific power q_Σ becomes small (see Fig. 12) and the contact heat transfer from the pin sample to the disc sample starts to predominate over the frictional heat generation. The temperature rise T_{IR} is even more lower, which is most probably attributed to the heat convection at the lateral surface of the pin sample.

Table 1
Dimensionless sliding duration Fo^*, time constant Θ and noise sensitivity Ω.

Thermocouple	Sliding duration $Fo^* = k t^*/h^2$	Time constant $\Theta = k\tau/h^2$	Noise sensitivity Ω due to Fig. 9
1	15	0.66	~13
2	2.8	0.12	~25

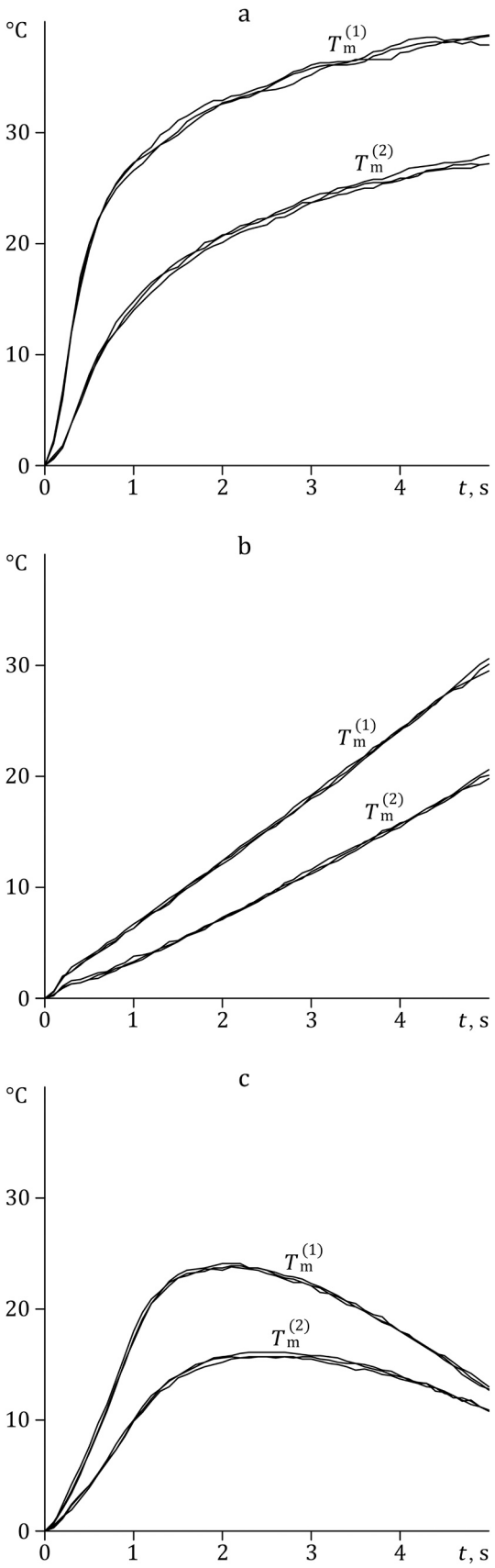

Fig. 14. Repeatability of the thermocouple temperatures $T_m^{(1)}$ and $T_m^{(2)}$: (a) velocity step; (b) acceleration; (c) deceleration.

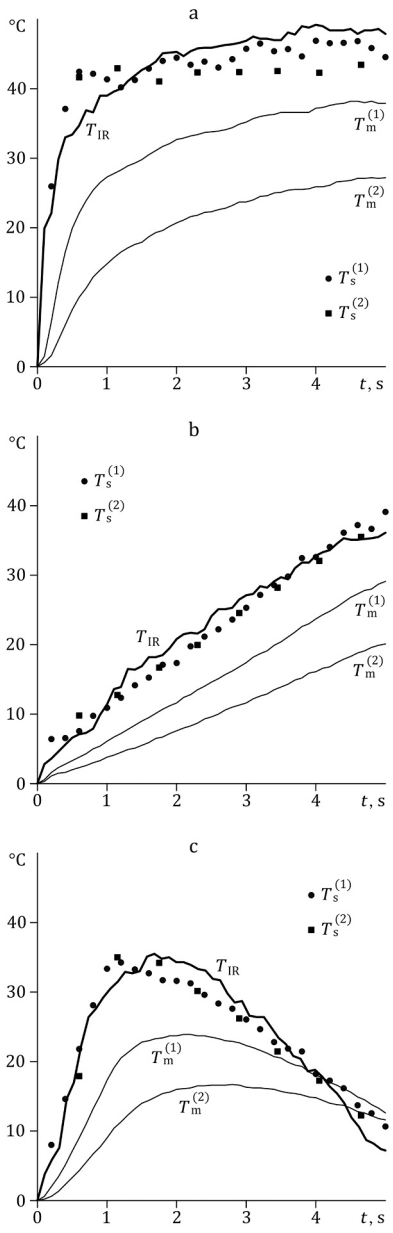

Fig. 15. Comparison of the thermocouple temperatures $T_m^{(1)}$ and $T_m^{(2)}$, infrared camera temperature rise T_{IR}, inverse surface temperatures $T_s^{(1)}$ and $T_s^{(2)}$: (a) velocity step; (b) acceleration; (c) deceleration.

Table 2
Degree of mismatch between the temperatures $T_s^{(1)}$, $T_s^{(2)}$, T_{IR}.

Sliding regime	MRAD between $T_s^{(1)}$ and $T_s^{(2)}$, %	MRAD between T_{IR} and $T_s^{(1)}$, %
Velocity step	6.2	4.7
Acceleration	5.2	6.1
Deceleration	6.3	7.1

The quantitative findings summarised in Table 2 allow concluding that $T_s^{(1)}$ and $T_s^{(2)}$ exhibit a good agreement between each other. MRAD between them is 5–6% for all sliding regimes. Such a small difference suggests that the experimental estimate of the time constant is sufficiently accurate. The inverse surface temperature $T_s^{(1)}$ enables predicting the contact temperature measured by infrared thermography with MRAD of 5–7%.

8. Conclusions

An inverse heat conduction problem was formulated to determine temperature at a sliding surface based on measurements by thermocouples taking account of their thermal inertia. The thermal behaviour of the thermocouples was simulated by a first-order model that incorporates a time constant parameter. The direct heat conduction problem was solved analytically using the Laplace integral transform approach, resulting in finding the kernel function given by Eq. (14). Parametric analysis of the obtained direct solution revealed the region of the heating duration and time constant in which the influence of the thermocouple thermal inertia is significant, as shown in Fig. 4. The inverse algorithm of Eqs. (14), (20) was developed based on the method of quadratures and natural step regularisation principle. The simulations showed that the noise sensitivity of the inverse algorithm is above 12. The inverse algorithm was applied to the problem of friction of a brake material against a steel. The experimental data were obtained on a pin-on-disc tribometer for three short-time regimes of sliding: velocity step, acceleration and deceleration. Temperature in the pin sample was measured by two identical miniature thermocouples installed at different small distances from the friction surface. The simulation and experimental results presented in Fig. 15 led to the following findings. The two inverse surface temperatures agree well for all sliding regimes. The difference between them makes up 5–6%. The sliding surface temperature predicted by the inverse algorithm deviates from that measured by infrared thermography by 5–7%.

CrediT authorship contribution statement

Oleksii Nosko: Supervision, Conceptualization, Formal analysis, Roles/Writing – original draft. **Yurii Tsybrii**: Methodology, Investigation, Writing – Review & Editing.

Funding

The present work was supported by the National Science Centre, Poland [grant number 2017/26/D/ST8/00142].

Declaration of Competing Interest

The authors declare that they have no known competing financial interests or personal relationships that could have appeared to influence the work reported in this paper.

References

[1] Liu T, Montefort J, Stanfield S, Palluconi S, Crafton J, Cai Z. Inverse heat transfer methods for global heat flux measurements in aerothermodynamics testing. Prog Aerosp Sci 2019;107:1–18.
[2] Agarwala S, Prabhu KN. An experimental approach based on inverse heat conduction analysis for thermal characterization of phase change materials. Thermochim Acta 2020;685:178540.
[3] Wang K, Wang G, Chen H, Wan S, Lv C. Quantitative identification of three-dimensional subsurface defect based on the fuzzy inference of thermal process. Int J Heat Mass Transf 2019;133:903–11.
[4] LeBreux M, Désilets M, Lacroix M. An unscented Kalman filter inverse heat transfer method for the prediction of the ledge thickness inside high-temperature metallurgical reactors. Int J Heat Mass Transf 2013;57:265–73.
[5] Taler J, Dzierwa P, Jaremkiewicz M, Taler D, Kaczmarski K, Trojan M, Sobota T. Thermal stress monitoring in thick walled pressure components of steam boilers. Energy 2019;175:645–66.
[6] Zhang J, Delichatsios MA. Determination of the convective heat transfer coefficient in three-dimensional inverse heat conduction problems. Fire Saf J 2009;44:681–90.
[7] Beck JV, Blackwell B, Clair St CR. Inverse heat conduction: Ill-posed problems. New York: Wiley-Interscience; 1985.
[8] Kennedy FE, Frusescu D, Li J. Thin film thermocouples arrays for sliding surface temperature measurement. Wear 1997;207:46–54.
[9] Nosko O, Tarasiuk W, Tsybrii Y, Nosko A, Senatore A, D'Urso V. Performance of acicular grindable thermocouples for temperature measurements at sliding contacts. Measurement 2021;181:109641.
[10] Chen WL, Yang YC, Chu SS. Estimation of heat generation at the interface of cylindrical bars during friction process. Appl Therm Eng 2009;29:351–7.
[11] Wang SK, Lee HL, Yang YC. Inverse problem of estimating time-dependent heat generation in a frictional heated strip and foundation. Int Commun Heat Mass Transf 2009;36:925–30.
[12] Quéméner O, Joly F, Neveu A. On-line heat flux identification from a rotating disk at variable speed. Int J Heat Mass Transf 2010;53:1529–41.
[13] Chen WL, Yang YC. Inverse prediction of frictional heat flux and temperature in sliding contact with a protective strip by iterative regularization method. Appl Math Model 2011;35:2874–86.
[14] Yang YC, Chen WL. A nonlinear inverse problem in estimating the heat flux of the disc in a disc brake system. Appl Therm Eng 2011;31:2439–48.
[15] Ghadimi B, Kowsary F, Khorami M. Heat flux on-line estimation in a locomotive brake disc using artificial neural networks. Int J Therm Sci 2015;90:203–13.
[16] Bauzin JG, Keruzore N, Laraqi N, Gapin A, Diebold JF. Identification of the heat flux generated by friction in an aircraft braking system. Int J Therm Sci 2018;130:449–56.
[17] Bauzin JG, Nguyen MN, Laraqi N, Cherikh MB. Thermal characterization of frictional interfaces using experiments and inverse heat conduction methods. Int J Therm Sci 2019;137:431–7.
[18] Woodbury KA. Effect of thermocouple sensor dynamics on surface heat flux predictions obtained via inverse heat transfer analysis. Int J Heat Mass Transf 1990;33(12):2641–9.
[19] Tagawa M, Ohta Y. Two-thermocouple probe for fluctuating temperature measurement in combustion – Rational estimation of mean and fluctuating time constants. Combust Flame 1997;109:549–60.
[20] Augustin S, Fröhlich T, Ament C, Güther T, Irrgang K, Lippmann L. Dynamic properties of contact thermometers for high temperatures. Measurement 2014;51:387–92.
[21] Frankel JI, Chen H. Analytical developments and experimental validation of a thermocouple model through an experimentally acquired impulse response function. Int J Heat Mass Transf 2019;141:1301–14.
[22] Doetsch G. Introduction to the theory and application of the Laplace transformation. Berlin: Springer; 1974.
[23] Carslaw HS, Jaeger JC. Conduction of heat in solids. 2nd ed. London: Oxford University Press; 1959.
[24] Stolz G. Numerical solutions to an inverse problem of heat conduction for simple shapes. J Heat Transf 1960;82:20–5.
[25] Beck JV. Surface heat flux determination using an integral method. Nucl Eng Des 1968;7(2):170–8.
[26] Alifanov OM. Inverse heat transfer problems. Berlin: Springer; 1994.